Curvature Index Failures in the Dynamics of an Electric Coupled Oscillator

Gustavo Revel Diego M. Alonso Jorge L. Moiola

Abstract— **In this work, the dynamics of an electric coupled oscillator is studied. The attention is centered on the first and second curvature indexes or Lyapunov coefficients of a Hopf bifurcation. The analysis is performed using the frequency domain method to calculate analytical expression of the indexes, and then establish the location of the first two curvature singularities. Numerical continuations are used to determine the dynamical behavior of the system in the vicinity of these points. A relatively complex structure of nested limit cycles was found near these degeneracies.**

I. Introduction

The curvature indexes, also known as Lyapunov coefficients or focal values, define the stability of a limit cycle emerging from a Hopf bifurcation. There are several ways to compute these coefficients, most of them reduce the system to the normal form of the Hopf bifurcation using different techniques (Poincaré normal forms, Lyapunov functions, power series expansion, etc., as shown in [1]–[4]). This task sometimes is cumbersome, especially in high dimensional systems [3]. An alternative method is given by the frequency domain approach which uses some well known techniques like harmonic balance, Nyquist stability criterium and state space formulations [5]–[7] to compute these indices. These tools are somewhat standard in electrical and electronics engineering.

In this article we analyze the dynamics of an electric oscillator using bifurcation theory. The attention is focused on computing Hopf bifurcations curves and the conditions leading to the first and second curvature index failures. The dynamical scenario emerging from these degeneracies (thoroughly analyzed in [2] and [8] using singularity theory) are obtained using AUTO [9]. Some global phenomena, including connections of cyclic fold bifurcations and cyclic cusp points are also described.

This work is organized as follows. In Section II a brief introduction to the frequency domain approach to analyze oscillations is given. In Section III the state space formulation of the electric circuit and its corresponding frequency domain representation are provided. The dynamics associated to the first and second curvature index failures is studied in Sections IV and V, respectively. Finally, some concluding remarks are given in Section VI.

The authors appreciate the financial support of UNS (PGI 24K/30), ANPCyT (PICT 11-12524) and CONICET (PIP 5032)

The authors are with Departamento de Ingeniería Eléctrica y de Computadoras, Universidad Nacional del Sur, Av. Alem 1253, B8000CPB Bahía Blanca, Argentina, and CONICET; grevel@uns.edu.ar.

II. Hopf bifurcation in the frequency domain

This section presents the basic concepts for the analysis of Hopf bifurcations using the frequency domain approach. The rigorous analysis is formulated in [5], [6].

Let us consider an n-dimensional nonlinear dynamical system described by

$$\dot{\mathbf{x}} = \mathbf{F}(\mathbf{x};\eta), \tag{1}$$

where $\mathbf{x} \in \mathbf{R}^n$ is the state vector, $\eta \in \mathbf{R}^p$ is the parameter vector and $\mathbf{F} : \mathbf{R}^n \times \mathbf{R}^p \mapsto \mathbf{R}^n$ is a smooth nonlinear vector field that satisfies $\mathbf{F}(\mathbf{0};\eta_0) = \mathbf{0}$.

The autonomous system (1) can be represented in feedback form with the linear part in the forward path and the nonlinear part in the feedback path, as

$$\begin{cases} \dot{\mathbf{x}} = \mathbf{A}\mathbf{x} + \mathbf{B}\mathbf{D}\mathbf{y} + \mathbf{B}\mathbf{u}, \\ \mathbf{y} = \mathbf{C}\mathbf{x}, \\ \mathbf{u} = \mathbf{g}(\mathbf{y};\eta) - \mathbf{D}\mathbf{y}, \end{cases} \tag{2}$$

where $\mathbf{A} \in \mathbf{R}^{n\times n}$ is the linear part of the original system, $\mathbf{g} : \mathbf{R}^m \times \mathbf{R}^p \mapsto \mathbf{R}^l$ is the nonlinear part, $\mathbf{B} \in \mathbf{R}^{n\times l}$, $\mathbf{C} \in \mathbf{R}^{m\times n}$ and $\mathbf{D} \in \mathbf{R}^{l\times m}$. Matrix $\mathbf{D}$ is arbitrary, revealing that there exist infinitely many equivalent feedback representations of (1). In addition, this extra degree of freedom can be used to obtain more suitable representations. Notice that all matrices may depend on η. The resulting multivariable feedback system is represented in Fig. 1a, where $\mathbf{v} \in \mathbf{R}^l$ is the input vector, $\mathbf{d} \in \mathbf{R}^m$ is a disturbance input and both are set to zero, $\mathbf{G}(s;\eta)$ is the transfer function matrix of the forward path defined as

$$\mathbf{G}(s;\eta) = \mathbf{C}[s\mathbf{I} - (\mathbf{A} + \mathbf{B}\mathbf{D}\mathbf{C})]^{-1}\mathbf{B}, \tag{3}$$

$\mathbf{f}(\mathbf{e};\eta)$ is the nonlinear part given by,

$$\mathbf{f}(\mathbf{e};\eta) = \mathbf{g}(\mathbf{y};\eta) - \mathbf{D}\mathbf{y}, \tag{4}$$

and $\mathbf{e} = -\mathbf{y}$.

The equilibrium point of the system is obtained solving

$$\mathbf{G}(0;\eta)\mathbf{f}(\mathbf{e};\eta) + \mathbf{e} = \mathbf{0}. \tag{5}$$

The Jacobian matrix of the nonlinear function $\mathbf{f}(\mathbf{e};\eta)$ evaluated at the equilibrium results

$$\mathbf{J}(\eta) = \left.\frac{\partial \mathbf{f}(\mathbf{e};\eta)}{\partial \mathbf{e}}\right|_{\mathbf{e}=\hat{\mathbf{e}}}. \tag{6}$$

A schematic representation of the linearized feedback scheme is shown in Fig. 1b.

Thus, if the open loop transfer function matrix $\mathbf{G}(i\omega;\eta)\mathbf{J}(\eta)$ has an eigenvalue at the critical point $-1 + i0$

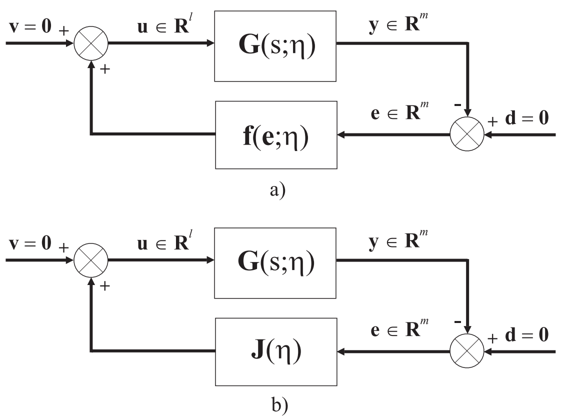

Fig. 1. Schematic representation of the feedback system. a) Nonlinear system. b) Linearized system.

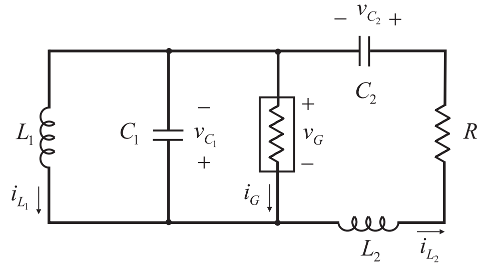

Fig. 2. Electric coupled oscillator.

for $\eta = \eta_0$ and $\omega = \omega_0$ ($\omega_0 \neq 0$), then a pair of eigenvalues of the closed loop system linearization assume the values $\pm i\omega_0$, setting the defining condition of a Hopf bifurcation. Then, generically, as the main bifurcation parameter η_i is varied, the equilibrium changes stability at $\eta_i = \eta_{i0}$ and a limit cycle emerges from it. The remaining parameters η_j, $j \neq i$ are auxiliary and fixed. In this framework, the graphical Hopf bifurcation method [5], [6] can be used to obtain an approximate solution of the limit cycle using well known techniques like harmonic balance method and Nyquist stability criterium. In addition, the method provides a way to derive analytical expressions for computing curvature indexes. The first and second curvature indexes, namely σ_1 and σ_2, formulas are given in the Appendix.

In the following we will use the notation H_{10} and H_{20} to indicate the first and second curvature index failures, respectively. The use of the notation H_{ij}, with $i, j = 0 \dots n$, is very common in the literature, where the subindex i indicate the number of curvature indexes that are zero and j denotes if there is a transversally degeneration of the Hopf bifurcation. By definition, $j = 0$ means that a simple pair of complex conjugate eigenvalues effectively cross the imaginary axis transversally.

III. Coupled electric oscillator

In this section the dynamics of a coupled electric circuit is analyzed using the frequency domain method. The schematic diagram of the oscillator is shown in Fig. 2 and is similar to the one studied in [10]–[12]. The mathematical model is easily obtained by simply applying the Kirchoff laws and setting the state variables: $x_1 = v_{C_1}$, $x_2 = i_{L_1}$, $x_3 = v_{C_2}$ and $x_4 = i_{L_2}$. In addition, the nonlinear element is characterized by the current-voltage $(i_G - v_G)$ relation $i_G = -\frac{1}{2}v_G - \frac{3}{5}v_G^2 + v_G^3$. The values of the remaining elements are: $C_1 = 1/\eta_1$, $C_2 = 1/(1+\sqrt{2})$, $L_1 = 1/\eta_3$, $L_2 = 1/(2-\sqrt{2})$ and $R = \eta_2$. The bifurcation parameters used here are η_1, η_2 and η_3, while the values of the rest of the components are chosen such that there is an irrational relation between the frequencies of oscillation. Therefore, the mathematical model of the electric oscillator is given by

$$\begin{cases} \dot{x}_1 = \eta_1 \left[\frac{1}{2}x_1 - \frac{3}{5}x_1^2 - x_1^3 + x_2 - x_4\right], \\ \dot{x}_2 = -\eta_3 x_1, \\ \dot{x}_3 = \left(1+\sqrt{2}\right) x_4, \\ \dot{x}_4 = \left(2-\sqrt{2}\right)\left[x_1 - x_3 - \eta_2 x_4\right]. \end{cases} \tag{7}$$

By inspection of (7) it is easy to see that the nonlinearity of the system is restricted to the first equation and depends only on x_1. As will be shown next, this fact greatly simplifies the representation of the system in the frequency domain, since the matrix $\mathbf{G}(s;\eta)$ results one-dimensional, and hence there is a unique eigenvalue. The feedback representation considered for (7) is

$$\mathbf{A} = \begin{bmatrix} 0 & \eta_1 & 0 & -\eta_1 \\ -\eta_3 & 0 & 0 & 0 \\ 0 & 0 & 0 & 1+\sqrt{2} \\ 2-\sqrt{2} & 0 & -2+\sqrt{2} & \left(-2+\sqrt{2}\right)\eta_2 \end{bmatrix}, \tag{8}$$

$$\mathbf{B} = \begin{bmatrix} 1 & 0 & 0 & 0 \end{bmatrix}^T, \tag{9}$$

$$\mathbf{C} = \begin{bmatrix} 1 & 0 & 0 & 0 \end{bmatrix}, \tag{10}$$

$$\mathbf{D} = \begin{bmatrix} 0 \end{bmatrix}, \tag{11}$$

$$\mathbf{u} = \mathbf{g}(y;\eta) - \mathbf{D}y = \eta_1 \left[\frac{1}{2}x_1 - \frac{3}{5}x_1^2 - x_1^3\right]. \tag{12}$$

In this case, the output is $y = -e = x_1$. The resulting expressions for the transfer function $\mathbf{G}(s;\eta)$ and the nonlinear function $\mathbf{f}(e;\eta)$ are

$$\mathbf{G}(s;\eta) = \tag{13}$$
$$\frac{s\left(s^2+\rho\eta_2 s+\sqrt{2}\right)}{s^4+\rho\eta_2 s^3+[\sqrt{2}+(\rho+\eta_3)\eta_1]s^2+\rho\eta_1\eta_2\eta_3 s+\sqrt{2}\eta_3\eta_1},$$

$$\mathbf{f}(e;\eta) = \eta_1\left[-\frac{1}{2}e - \frac{3}{5}e^2 + e^3\right], \tag{14}$$

where $\rho = 2-\sqrt{2}$. From (5), the equilibrium point is $\hat{e} = 0$, since $\mathbf{G}(s;\eta)$ has a zero at $s = 0$. The Jacobian results in

$$\mathbf{J}(\eta) = \left.\frac{\partial \mathbf{f}(e;\eta)}{\partial e}\right|_{e=0} = -\frac{1}{2}\eta_1. \tag{15}$$

Since $\mathbf{G}(s;\eta)$ and $\mathbf{J}(\eta)$ are scalar quantities, the open loop transfer function $\mathbf{G}(s;\eta)\mathbf{J}(\eta)$ has an unique eigenvalue given by

$$\hat{\lambda}(\omega;\eta) = \left.\mathbf{G}(s;\eta)\mathbf{J}(\eta)\right|_{s=i\omega}. \tag{16}$$

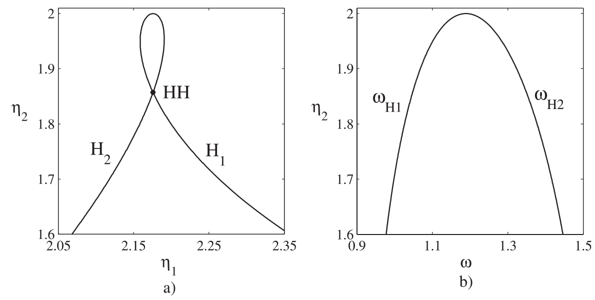

Fig. 3. Hopf bifurcation in the electric coupled oscillator ($\eta_3 = 0.65$). a) Hopf curve. b) Frequency of oscillation.

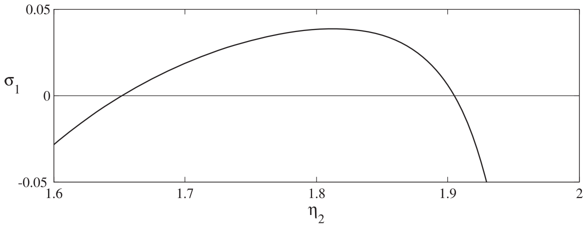

Fig. 4. Plot of the first curvature index σ_1 versus η_2 for $\eta_3 = 0.65$.

Therefore, the Hopf bifurcation points are obtained solving

$$\begin{cases} \Re\{\hat{\lambda}\} = -1, \\ \Im\{\hat{\lambda}\} = 0. \end{cases} \tag{17}$$

In this particular case, it is easy to obtain the critical values of η_1 and the frequency of the oscillation ω_0 in terms of η_2 and η_3. The resulting formulas are very extensive to be included in this paper, but they are not difficult to obtain using any symbolic math software. The solution obtained for $\eta_3 = 0.65$ are shown in Fig. 3. As seen on Fig. 3a, the Hopf bifurcation curve is divided in two branches, namely H_1 and H_2 and both intersect at a Hopf-Hopf bifurcation (also called double Hopf) point (HH at $\eta_1 = 2.17571$ and $\eta_2 = 1.85708$). A plot of the frequency of the emerging limit cycle from the Hopf bifurcation is shown on Fig. 3b, where ω_{H_1} is associated with H_1 and ω_{H_2} with H_2. Notice that both frequencies coincide at the maximum point of the Hopf curve and are different for the Hopf-Hopf point.

Hopf-Hopf bifurcation explains the appearance of quasiperiodic oscillations in this circuit. At least four cases related to the unfolding of the truncated normal form [13] of the Hopf-Hopf bifurcation can be recognized in the parameter plane $\eta_1 - \eta_2$ for different values of η_3. Three of them belong to the simple cases (2D quasiperiodic oscillations or tori) and the remaining one to the complex cases (2D and 3D tori). These phenomena as well as the location of a fold-flip bifurcation of periodic orbits, for a similar circuit can be seen in [12]. The transition from simple to complex scenarios is related to the failure of the first curvature index of H_1. This singularity is analyzed in the next section.

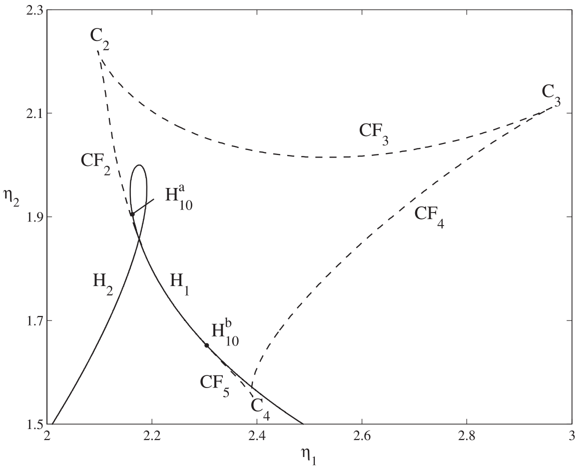

Fig. 5. Bifurcation diagram for $\eta_3 = 0.65$. Global scenario.

IV. First curvature index failure, H_{10}

The H_{10} singularity occurs when the first curvature index of a Hopf bifurcation becomes zero, this situation is also known in the literature as generalized Hopf or Bautin bifurcation [13]. The common techniques used to study this singularity are Poincaré normal forms, Lyapunov functions, power series expansion, etc. In this work we use the frequency domain approach described in Section II. The formula to compute σ_1 is given in the Appendix. Then, using (18) and replacing the parameter values and frequency corresponding to the Hopf bifurcation curve [i.e. the solution of (17)], the value of the curvature index is obtained. The plot of σ_1 versus η_2 is shown in Fig. 4. Notice that there are two crossings by zero, which means that there is a couple of H_{10} singularities. The first curvature failure H^a_{10} is located at $(\eta_1, \eta_2) = (2.16308, 1.90484)$, while the second failure H^b_{10} is at $(\eta_1, \eta_2) = (2.30433, 1.65203)$. The results obtained with the frequency domain method were confirmed using the continuation programs AUTO and MATCONT [14].

It is well known that a cyclic fold bifurcation curve emerges from this singularity [13]. The curves arising in both generalized Hopf points are connected through a complex structure of cyclic fold (CF) bifurcations and cuspidal points (C), as shown in the continuation diagram of Fig. 5 for $\eta_3 = 0.65$. The local scenarios around H^a_{10} and H^b_{10} are shown in Figs. 6 and 7, respectively. The dynamical behavior of the system around the point H^a_{10} (the situation is analogous for H^b_{10}) is better described if a couple of cross-sections above and below the singularity are made. The bifurcation diagrams varying η_1 for $\eta_2 = 1.92$ (above H^a_{10}) and $\eta_2 = 1.88$ (below H^a_{10}) are shown in Figs. 8a and 8b, respectively. There, the dashed lines represent unstable equilibria and unstable cycles and the solid lines are stable equilibria and stable cycles.

Starting with the bifurcation diagram for $\eta_2 = 1.92$ (Fig. 8a), the equilibrium undergoes a supercritical Hopf bifurcation H_1^- (the first curvature index is negative), then the limit cycle is stable and increases its amplitude towards

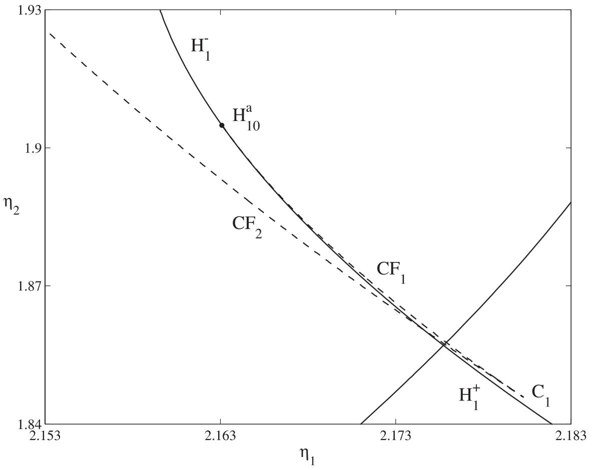

Fig. 6. Detailed view of the singularity H_{10}^{a}.

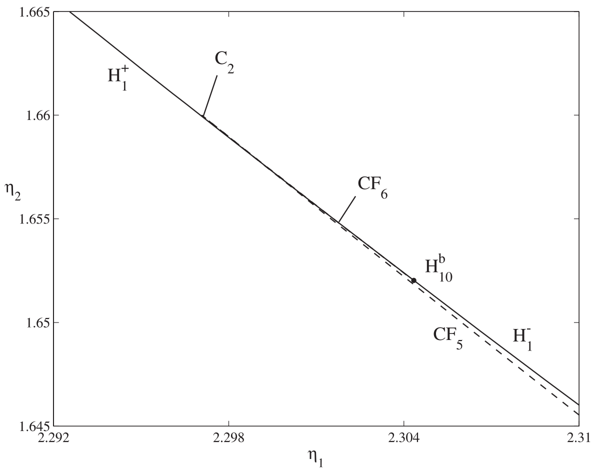

Fig. 7. Detailed view of the singularity H_{10}^{b}.

the left (decreasing values of η_1). The stable limit cycle collapses with an unstable cycle at CF_2. This phenomenon is not associated directly with the first curvature index failure.

The situation for $\eta_2 = 1.88$ (Fig. 8b) is quite different. The equilibrium point exhibits a subcritical Hopf bifurcation H_1^+, since the curvature index becomes positive due to H_{10}^{a}. Then, the limit cycle is unstable and increases its amplitude towards the right until it collapses with a stable limit cycle at CF_1. This cyclic fold bifurcation is in direct relation with H_{10}^{a}. The stable limit cycle increases its amplitude and coalesces with an unstable cycle at CF_2. Notice that there is a range of values of η_1 where three cycles coexist. This situation is similar to that occurring in the vicinity of the second curvature index failure, but as will be shown next, CF_2 is not related to H_{20}.

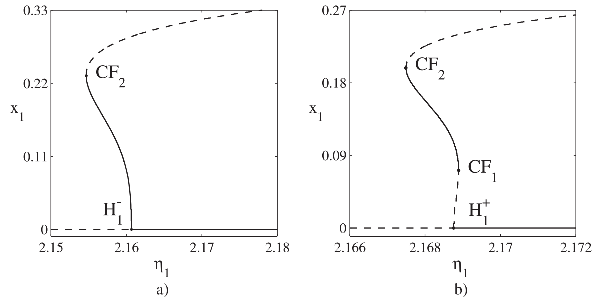

Fig. 8. Dynamical scenario near H_{10}^{a} ($\eta_3 = 0.65$). a) Bifurcation diagram for $\eta_2 = 1.92$. b) Bifurcation diagram for $\eta_2 = 1.88$.

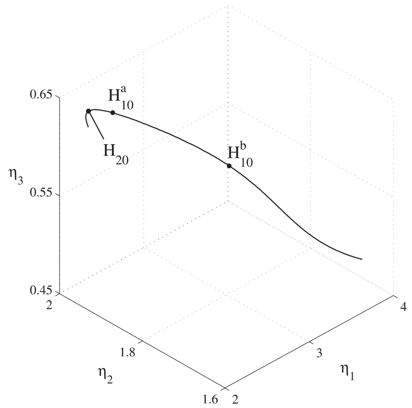

Fig. 9. Curve of H_{10} singularities varying the parameters η_1, η_2 and η_3 simultaneously.

V. Second curvature index failure, H_{20}

The second curvature index failure is obtained when both Lyapunov coefficients are simultaneously zero, i.e., $\sigma_1 = \sigma_2 = 0$ and the singularity is denoted as H_{20}. In this complex co-dimension three phenomenon, a curve of cyclic cusp bifurcations emerges from the point H_{20}, instead of the cyclic fold curve arising in the H_{10} bifurcation, so there are expected to exist up to three limit cycles in a neighborhood of this singularity. Furthermore, in this case, three bifurcation parameters need to be varied (η_1, η_2 and η_3) to locate this degeneracy. To detect the second index failure it is necessary to obtain the points of the parameter space where $\sigma_1 = 0$. This task was performed numerically using LOCBIF [15], resulting in the curve of H_{10} bifurcations shown in Fig. 9. Obviously these points satisfy the conditions of the Hopf bifurcations and thus the corresponding frequency can be obtained from (17). Then σ_2 is computed using (19) for the parameter values where $\sigma_1 = 0$, and a H_{20} singularity was detected at $(\eta_1, \eta_2, \eta_3) = (2.235, 1.978, 0.631)$.

The unfolding of the H_{20} singularity on the parameter plane $\eta_2 - \eta_3$ is shown in Fig. 10 and the corresponding bifurcation diagrams that describe the dynamical behavior of the system around this singular point are shown in Fig. 11.

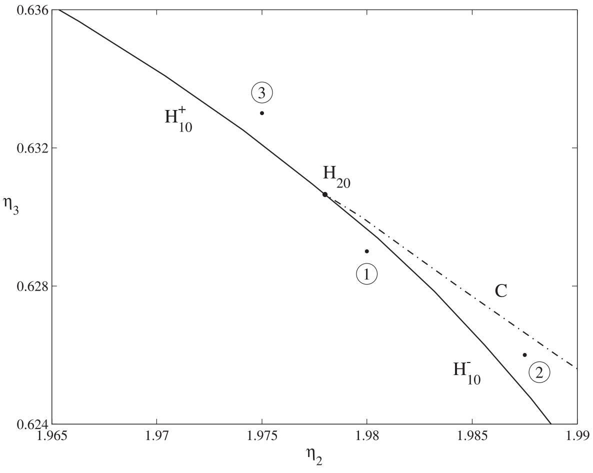

Fig. 10. Unfolding of the H_{20} bifurcation.

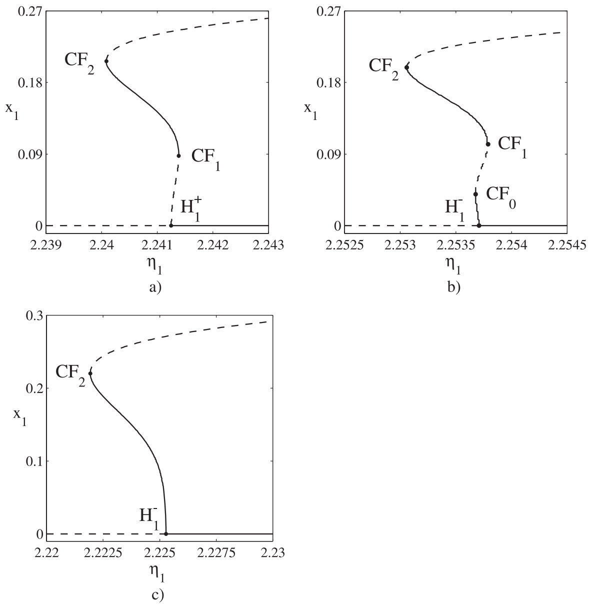

Fig. 11. Dynamics around the H_{20} singularity. a) Bifurcation diagram varying η_1 in region 1 ($\eta_2 = 1.980$, $\eta_3 = 0.629$). b) Region 2 ($\eta_2 = 1.9875$, $\eta_3 = 0.626$). c) Region 3 ($\eta_2 = 1.975$, $\eta_3 = 0.633$).

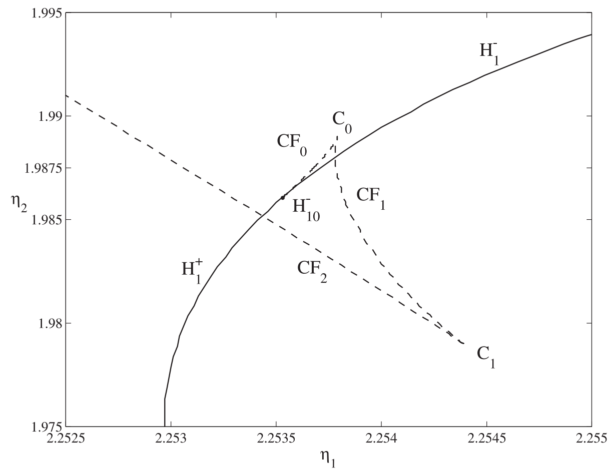

Fig. 12. Bifurcation diagram for $\eta_3 = 0.626$.

Figure 10 is obtained projecting the H_{10} curve in the plane $\eta_2 - \eta_3$. The H_{20} point divides the H_{10} curve in two, namely H_{10}^+ and H_{10}^- according to the sign of the second curvature index. Basically this singularity splits the parameter space in three regions with different dynamical phenomena. In order to describe the dynamical behavior of the system in a neighborhood of the H_{20} point, continuation diagrams are obtained varying η_1 for values of η_2 and η_3 fixed.

Setting $\eta_2 = 1.980$ and $\eta_3 = 0.629$ (region 1 in Fig. 10) the diagram of Fig. 11a is obtained. An unstable limit cycle, born at the Hopf bifurcation H_1^+, collides with a stable cycle at CF_1. This stable cycle suffers another cyclic fold bifurcation at CF_2 where it collapses with an unstable cycle. This phenomenon is global and does not belong to the local unfolding.

The dynamics associated to region 2 is shown in Fig. 11b. The Hopf bifurcation becomes supercritical since the curve H_{10}^- is crossed, so the limit cycle is now stable and grows its amplitude towards the left until it suffers the cyclic fold bifurcation CF_0 with an unstable limit cycle. This unstable cycle collides with a stable limit cycle at CF_1. This last cycle collapses with the global bifurcation CF_2 as before. Therefore, in this region at least three nested limit cycle surrounding the equilibrium point do exist (actually there are more cycles due to global bifurcations not directly associated with the H_{20} singularity).

The situation becomes far more simple in region 3 (Fig. 11c), since both cyclic fold bifurcations CF_0 and CF_1 disappear in a cusp point when crossing the curve C from region 2 to 3 (see Fig. 10). Therefore, in region 3 there is only a stable limit cycle that emanates towards the left from the supercritical Hopf bifurcation H_1^-. Again, this cycle disappears due to the global cyclic fold CF_2.

The transition from region 3 back to region 1 is characterized by a change in the stability of the limit cycle emerging from the Hopf bifurcation, that becomes unstable (when crossing H_{10}^+) and grows towards the right until it vanishes at the cyclic fold bifurcation CF_1, as explained before.

It is interesting to notice the change in the bifurcation structure in the neighborhood of H_{10} due to the second curvature index failure. Toward this end, the continuation diagram in the parameter plane $\eta_1 - \eta_2$ for $\eta_3 = 0.626$ is derived and is shown in Fig. 12. Notice that the scenarios for $\eta_2 = 1.985$, 1.9875 and 1.99 can be associated to those on Figs. 11a, b and c, respectively.

Finally, the location of the second curvature index failure was confirmed using MATCONT, since this program calculates numerically the value of the second Lyapunov coefficient every time a generalized Hopf bifurcation is found.

VI. CONCLUSIONS

The frequency domain method provides analytical closed form expressions to calculate the curvature indexes. These expressions might become more or less complicated depending on the system nonlinearity. In the case studied here, the formulas have been easily obtained, since the nonlinearity depends only on one variable of the system.

In this work we combine the analytic power of the frequency domain approach of the Hopf bifurcation with the numerical continuation results to describe the complexity of multiple curvature failures involving up to three limit cycles in the unfolding of certain organizing centers of the dynamics.

APPENDIX

CURVATURE INDEX FORMULAS

The expressions of the first and second curvature indexes in the frequency domain are [6], [7]

$$\sigma_1 = -\Re\left\{\frac{\mathbf{w}^T\mathbf{G}(i\omega)\mathbf{p_1}}{\mathbf{w}^T\mathbf{G}'(i\omega)\mathbf{J}\mathbf{V_{11}}}\right\} = -\Re\{\gamma_1\}, \tag{18}$$

$$\begin{aligned}\sigma_2 = -\Re\Bigg\{\frac{\mathbf{w}^T}{\mathbf{w}^T\mathbf{G}'(i\omega)\mathbf{J}\mathbf{V_{11}}}\Bigg[&-\gamma_1\mathbf{G}'(i\omega)(\mathbf{J}\mathbf{V_{13}}+\mathbf{p_1}) \\ &-\gamma_1\mathbf{G}(i\omega)\mathbf{p_1}' + \frac{1}{2}\gamma_1^2\mathbf{G}''(i\omega)\mathbf{J}\mathbf{V_{11}} + \mathbf{G}(i\omega)\mathbf{p_2}\Bigg]\Bigg\},\end{aligned} \tag{19}$$

where

$$\begin{aligned}
\mathbf{G}'(i\omega) &= \left.\frac{d\mathbf{G}(s)}{ds}\right|_{s=i\omega}, \quad \mathbf{G}''(i\omega) = \left.\frac{d^2\mathbf{G}(s)}{ds^2}\right|_{s=i\omega},\\
\mathbf{p_1} &= D_2\left[\frac{1}{2}\bar{\mathbf{V}}_{\mathbf{11}}\mathbf{V_{22}} + \mathbf{V_{11}}\mathbf{V_{02}}\right] + \frac{1}{8}D_3\mathbf{V_{11}^2}\bar{\mathbf{V}}_{\mathbf{11}},\\
\mathbf{p_1}' &= \frac{d\mathbf{p_1}(s)}{ds},\\
\mathbf{p_2} &= \frac{D_2}{2}\left[2\mathbf{V_{11}}\mathbf{V_{04}} + 2\mathbf{V_{02}}\mathbf{V_{13}} + \bar{\mathbf{V}}_{\mathbf{22}}\mathbf{V_{33}}\right.\\
&\quad \left.+ \bar{\mathbf{V}}_{\mathbf{11}}\mathbf{V_{24}} + \bar{\mathbf{V}}_{\mathbf{13}}\mathbf{V_{22}}\right] + \frac{D_3}{8}\left[4\mathbf{V_{11}}\mathbf{V_{02}^2}\right.\\
&\quad + \mathbf{V_{11}^2}\bar{\mathbf{V}}_{\mathbf{13}} + \bar{\mathbf{V}}_{\mathbf{11}}^{\mathbf{2}}\mathbf{V_{33}} + 4\bar{\mathbf{V}}_{\mathbf{11}}\mathbf{V_{02}}\mathbf{V_{22}}\\
&\quad \left.+ 2\mathbf{V_{11}}\mathbf{V_{22}}\bar{\mathbf{V}}_{\mathbf{22}} + 2\mathbf{V_{11}}\bar{\mathbf{V}}_{\mathbf{11}}\mathbf{V_{13}}\right]\\
&\quad + \frac{D_4}{48}\left[\mathbf{V_{11}^3}\bar{\mathbf{V}}_{\mathbf{22}} + 6\mathbf{V_{11}^2}\bar{\mathbf{V}}_{\mathbf{11}}\mathbf{V_{02}}\right.\\
&\quad \left.+ 3\mathbf{V_{11}}\bar{\mathbf{V}}_{\mathbf{11}}^{\mathbf{2}}\mathbf{V_{22}}\right] + \frac{D_5}{192}\mathbf{V_{11}^3}\bar{\mathbf{V}}_{\mathbf{11}}^{\mathbf{2}},\\
\mathbf{H}(s) &= [\mathbf{I} + \mathbf{G}(s)\mathbf{J}]^{-1}\mathbf{G}(s),\\
\mathbf{V_{02}} &= -\frac{\mathbf{H}(0)}{4}D_2\mathbf{V_{11}}\bar{\mathbf{V}}_{\mathbf{11}},\\
\mathbf{V_{22}} &= -\frac{\mathbf{H}(2i\omega)}{4}D_2\mathbf{V_{11}^2},\\
\mathbf{V_{33}} &= -\frac{\mathbf{H}(3i\omega)}{4}\left\{2D_2\mathbf{V_{11}}\mathbf{V_{22}} + \frac{1}{6}D_3\mathbf{V_{11}^3}\right\},\\
\mathbf{V_{04}} &= -\frac{\mathbf{H}(0)}{4}\Bigg\{D_2\left[2\mathbf{V_{02}^2} + \mathbf{V_{22}}\bar{\mathbf{V}}_{\mathbf{22}}\right.\\
&\quad \left.+ \bar{\mathbf{V}}_{\mathbf{11}}\mathbf{V_{13}} + \mathbf{V_{11}}\bar{\mathbf{V}}_{\mathbf{13}}\right] + \frac{D_3}{4}\left[\mathbf{V_{11}^2}\bar{\mathbf{V}}_{\mathbf{22}}\right.\\
&\quad \left.+ \bar{\mathbf{V}}_{\mathbf{11}}^{\mathbf{2}}\mathbf{V_{22}} + 4\mathbf{V_{11}}\bar{\mathbf{V}}_{\mathbf{11}}\mathbf{V_{02}}\right] + \frac{D_4}{16}\mathbf{V_{11}^2}\bar{\mathbf{V}}_{\mathbf{11}}^{\mathbf{2}}\Bigg\},\\
\mathbf{V_{24}} &= -\frac{\mathbf{H}(2i\omega)}{4}\Bigg\{2D_2\left[2\mathbf{V_{02}}\mathbf{V_{22}} + \bar{\mathbf{V}}_{\mathbf{11}}\mathbf{V_{33}}\right.\\
&\quad \left.+ \mathbf{V_{11}}\mathbf{V_{13}}\right] + D_3\left[\mathbf{V_{11}^2}\mathbf{V_{02}} + \mathbf{V_{11}}\bar{\mathbf{V}}_{\mathbf{11}}\mathbf{V_{22}}\right]\\
&\quad + \frac{D_4}{12}\mathbf{V_{11}^3}\bar{\mathbf{V}}_{\mathbf{11}}\Bigg\},
\end{aligned}$$

where $\mathbf{V_{11}}$ and $\mathbf{w}$ are the right and left eigenvectors of the matrix $\mathbf{G}(i\omega)\mathbf{J}$, ω is the frequency at the Hopf bifurcation, D_i indicate the ith partial derivative evaluated at the equilibrium $\hat{\mathbf{e}}$, and $\mathbf{V_{13}}$ is calculated solving

$$\begin{aligned}(\mathbf{I} - \mathbf{V_{11}}\mathbf{V_{11}}^T)[\mathbf{I} + \mathbf{G}(i\omega)\mathbf{J}]\mathbf{V_{13}} &= \\ -(\mathbf{I} - \mathbf{V_{11}}\mathbf{V_{11}}^T)\mathbf{G}(i\omega)\mathbf{p_1}&,\end{aligned}$$

with the restriction $\mathbf{V_{11}} \perp \mathbf{V_{13}}$.

Notice that in this particular case $\mathbf{V_{13}} = 0$ since $\mathbf{V_{11}} = 1$. In addition, $\mathbf{V_{02}} = \mathbf{V_{04}} = 0$ since $\mathbf{G}(0) = 0$ (then $\mathbf{H}(0) = 0$). These facts simplify greatly the calculations of the remaining vectors used to obtain the expressions of the curvature indexes.

REFERENCES

[1] B. D. Hassard and Y. H. Wan, "Bifurcation formulae derived from center manifold theory," *Journal of Mathematical Analysis and Applications*, vol. 63, pp. 297–312, 1978.

[2] M. Golubitsky and W. F. Langford, "Classification and unfoldings of degenerate Hopf bifurcations," *Journal of Differential Equations*, vol. 41, pp. 375–415, 1981.

[3] W. Farr, C. Li, I. S. Labouriau, and W. F. Langford, "Degenerate Hopf bifurcation formulas and Hilbertt's 16th problem," *SIAM Journal on Mathematical Analysis*, vol. 20, no. 1, pp. 13–20, 1989.

[4] Y. A. Kuznetsov, "Numerical normalization techniques for all codim 2 bifurcations of equilibria in ODE's," *SIAM Journal of Numerical Analysis*, vol. 36, no. 4, pp. 1104–1124, 1999.

[5] A. I. Mees and L. O. Chua, "The Hopf bifurcation theorem and its applications to nonlinear oscillations in circuits and systems," *IEEE Trans. on Circuits and Systems*, vol. 26, no. 4, pp. 235–254, 1979.

[6] A. I. Mees, *Dynamics of Feedback Systems*. Chichester, UK: John Wiley & Sons, 1981.

[7] J. L. Moiola and G. Chen, *Hopf Bifurcation Analysis. A Frequency Domain Approach*. Singapore: World Scientific, 1996.

[8] M. Golubitsky and D. G. Schaeffer, *Singularities and Groups in Bifurcation Theory, I*. New York: Springer-Verlag, 1985.

[9] E. J. Doedel, R. C. Paffenroth, A. R. Champneys, T. F. Fairgrieve, Y. A. Kuznetsov, B. E. Oldeman, B. Sandstede, and X.-J. Wang, "AUTO2000: Continuation and bifurcation software for ordinary differential equations (with HomCont)," California Institute of Technology, Pasadena, California USA, Tech. Rep., 2002.

[10] P. Yu, "Analysis on double Hopf bifurcation using computer algebra with the aid of multiple scales," *Nonlinear Dynamics*, vol. 27, pp. 19–53, 2002.

[11] G. R. Itovich and J. L. Moiola, "Double Hopf bifurcation analysis using frequency domain methods," *Nonlinear Dynamics*, vol. 39, pp. 235–258, 2005.

[12] G. Revel, D. M. Alonso, and J. L. Moiola, "A gallery of oscillations in a resonant electric circuit: Hopf-Hopf and fold-flip interactions." *Intnl. Journal of Bifurcation and Chaos, in press 2007, to appear*, 2008.

[13] Y. A. Kuznetsov, *Elements of Applied Bifurcation Theory*. New York: Springer-Verlag, 2004.

[14] A. Dhooge, W. Govaerts, Y. A. Kuznetsov, W. Mestrom, A. Riet, and B. Sautois, "MATCONT and CL_MATCONT: Continuation toolboxes in MATLAB," Universiteit Gent, Belgium, Tech. Rep., 2006.

[15] A. I. Khibnik, Y. A. Kuznetsov, V. V. Levitin, and E. V. Nikolaev, "LOCBIF, Interactive LOCal BIFurcation Analyzer. Version 2," Tech. Rep., 1992.